RSC Advances

ROYAL SOCIETY OF CHEMISTRY

www.rsc.org/advances

Journal Name

ARTICLE

Unusual Anti-Bacterial Behavior and Corrosion Resistance of Magnesium Alloy Coated with Diamond-Like Carbon

Received 00th January 20xx,
Accepted 00th January 20xx

DOI: 10.1039/x0xx00000x

www.rsc.org/

Hongqing Feng[a], Xiaolin Zhang[a], Guosong Wu[a], Weihong Jin[a], Qi Hao[a, b], Guomin Wang[a], Yifan Huang[a], and Paul K. Chu*[a]

Magnesium and magneisum alloys are promising materials in degradable biomedical implants and also have inherent anti-bacterial ability. A surface coating can reduce the surface corrosion rate of magnesium-based materials without compromising the anti-bacterial property. In this work, diamond-like carbon (DLC) caotings are deposited on the AZ31 Mg alloy by one-step plasma immersion ion implantation and deposition (PIII&D). After PIII&D, The corrosion current density diminishes largely from 3.17×10^{-4} A/cm^2 to 6.53×10^{-5} A/cm^2. The pH and amounts of leached magnesium ions are also significantly reduced. Meanwhile, 3×10^4 bacteria seeded on the AZ31-DLC are completely annihilated within 6 hours in contrast to 5×10^3 live ones left on the untreated AZ31 and more than 6×10^8 on Si-DLC (DLC deposited on Si). The favorable anti-bacteria behavior of AZ31-DLC is attributed to the combined effects of favorable bacteria adhesion on the DLC surface and local release of hydroxyl and magnesium ions from the magnesium substrate *via* defects in the DLC films.

1. Introduction

Magnesium and magnesium alloys have attracted much attention in the biomedical field in recent years[1–3] because of their unique biodegradable properties which can be exploited to avoid a follow-up surgery after tissue healing. In addition, the inherent anti-bacterial ability arising from release of magnesium ions and increased alkalinity bodes well for orthopedic, dental, and cardiovascular applications.[4] However, since the degradation rate of magnesium alloys tends to be too high in the physiological environment, anti-corrosion methods have been proposed to mitigate surface degradation.[5–8] Taking all the factors into consideration, it is important to enhance the corrosion resistance while not compromising the anti-bacterial capability of the magnesium alloys.[9,10]

Diamond-like carbon (DLC), a metastable form of amorphous carbon containing a significant fraction of sp^3 bonds,[11,12] have many applications including coatings for implants[13,14]. For example, DLC coatings deposited on NiTi alloys increase cell proliferation[15] and blood compatibility.[16] However, conventional DLC coatings do not adhere well to magnesium-based materials because of the large internal stress resulting from sp^3 bonds. In this respect, plasma immersion ion implantation and deposition (PIII&D)[17] has been utilized to increase the bonding strength because energetic ion bombardment induces nucleation and inter-diffusion between the film and substrate . Multiple-layer[18,19] and single-layer[20–23] DLC coatings have been prepared on magnesium alloys and improved their anti-corrosion ability.

Besides the corrosion resistance, the anti-bacterial properties of Mg and Mg alloys are very important in order to minimize post-surgery infection. However, the anti-bacterial capability of DLC-coated magnesium alloys has seldom been evaluated. This is because DLC being quite inert is not expected to produce substantial antibacterial effects and it may even reduce the anti-bacterial effects rendered by the Mg substrate. Silver-doped DLC[24] has been reported to have some anti-bacterial effects on stainless steels,[25,26] but the reduction of bacteria colony forming units (CFU) is within 2 orders of magnitudes, and the inactivation is observed to be localized in the surface area. In this work, DLC is deposited on AZ31 Mg alloy by PIII&D in one simple step and the anti-bacterial behaviour of the DLC-coated AZ31 Mg alloy is investigated systematically. The bacteria killing rate is unexpectedly much faster than that observed from the substrate and the Ag-doped DLC coatings in other studies [25,26]. The mechanism is studied and proposed.

2. Experimental Details

2.1 Sample preparation and treatment

Specimens with dimensions of 10 mm × 10 mm × 5 mm were cut from a commercial extruded AZ31 (Mg – 3.0 wt. % AL – 0.1 wt. % Zn) alloy rod. Prior to plasma surface modification, the samples were mechanically ground by up to # 1200 sand paper and ultrasonically cleaned in alcohol. PIII&D was conducted on the GPI-100 ion implanter in the Plasma Laboratory of City University of Hong Kong. After the vacuum chamber was evacuated to $3\text{x}10^{-3}$ Pa, acetylene (C_2H_2) was introduced at a flow rate of 30 sccm to

[a] Department of Physics and Materials Science, City University of Hong Kong, Tat Chee Avenue, Kowloon, Hong Kong, China
[b] Department of Physics and Jiangsu Key Laboratory for Advanced Metallic Materials, Southeast University, Nanjing 211189, China.
* Corresponding author electronic mail: paul.chu@cityu.edu.hk (P. K. Chu).

establish a working pressure of $3x10^{-1}$ Pa. A 1 kW 13.56 MHz RF generator was used to trigger the plasma. Negative high-voltage pulses (-20 kV) with a pulse width of 50 µs and frequency of 50 Hz produced by a power modulator were applied to the samples to conduct PIII&D for 2 h without additional sample heating. Silicon wafers were processed under the same conditions for comparison.

2.2 Surface characterization

Raman scattering (514.5 nm argon laser, HR LabRAM) and scanning electron microscopy (SEM) were performed to characterize the DLC films. Contact angle measurements were performed using 4 µL water and diiodomethane (CH_2I_2) droplets (Model 200, Ramé-Hart, USA) at room temperature and the average value was calculated from three measurements. The surface free energy was calculated by the Owens-Wendt geometric mean method. The surface free energy between a liquid and solid has the following relationship:

$$\gamma_S = \gamma_S^d + \gamma_S^p \quad \text{and} \quad (1)$$

$$\gamma_L(\cos\emptyset+1) = 2[(\gamma_S^d\gamma_L^d)^{1/2}+(\gamma_S^p\gamma_L^p)^{1/2}] , \quad (2)$$

where Ø is the contact angle of the solid surface with the liquid, γ_S is the surface free energy of the solid, γ_S^d and γ_S^p represent the dispersive component and polar component of the solid, γ_L is the surface energy of the liquid, and γ_L^d and γ_L^p represent the dispersive component and polar component of the liquid. The values of γ_L, γ_L^d, and γ_L^p of water are 72.8, 22.1 and 50.7 mN/m, respectively and those of γ_L, γ_L^d, and γ_L^p of CH_2I_2 are 50.8, 50.4, and 0.4 mN/m, respectively.

2.3 Corrosion study: electrochemical tests, morphology observation, pH and magnesium ion release

Electrochemical experiments were carried out on a Zahner Zennium electrochemical workstation in accordance with the three-electrode technique in Lysogeny broth (LB) medium. The potential was referenced to a saturated calomel electrode (SCE) and the counter electrode was a platinum sheet. The specimen with a surface area of 10 × 10 mm^2 was exposed to the LB solution and after immersion for 5 min, electrochemical impedance spectra (EIS) were acquired. The data were recorded from 100 kHz to 100 mHz with a 5 mV sinusoidal perturbation signal at the open-circuit potential. The potential was scanned from the cathodic to anodic regions at a rate of 1 mV/s from -300 to 600 mV to obtain the polarization curves.

100 µL of the LB medium were put on the samples and incubated at 37 °C for 0h, 3h and 6 h. After corrosion, the samples were washed in ethonal, and then dried in an oven at 37 ℃ for 1 day and observed by scanning electron microscopy (SEM, JSM-820, JEOL Ltd., Japan). To avoid medium loss due to evaporation, the gaps between the wells were filled with distilled water.

100 µL of the LB medium were placed and collected from each sample in 6 hours. The pH of the 100 µL LB medium on the surface was measured by a mini pH monitor (CLEAN L'EAU PH30, USA) capable of measuring a very small amount of liquid down to 30 µL.

The collected LB medium was diluted 20 times and 1 mL was taken to measure the concentration of the leached magnesium ions by inductively-coupled plasma optical emission spectroscopy (ICP-OES, PE Optima 2100DV, Perkin Elmer, USA). The magnesium ion concentrations were calculated according to the standard curve and QA/QC tests were carried out for every 20 analyses.

2.4 Anti-bacterial properties: planktonic and adherent bacteria viability

The bacteria *Staphylococcus aureus (S. au)* were used to evaluate the disinfection effectiveness and anti-bacterial behavior of the samples. The specimens were first sterilized in 70% ethanol for 30 min. The bacteria in the frozen stock were cultured in the LB medium at 37 ℃ overnight, diluted to OD_{600} = 0.10, and cultured for an additional 1 hour to OD_{600} = 0.2 (1.5×10^9 /mL). The bacteria were diluted 5,000 times with the LB medium and 100 µL of the medium were placed on the samples on 24-well plates. The total amount of bacteria was 3×10^4 colony forming units (CFU) initially. The control was cultured directly on polystyrene on 24 well-plates in pure LB. After 3 and 6 h, the planktonic bacteria in the LB medium were collected, serially diluted 10 folds, and spread on LB agar to perform CFU counting after culturing for 12 hours. To avoid medium loss from evaporation, the gaps between wells were filled with distilled water. The 6-hour culture solution on the AZ31-DLC surface was spread on agar without dilution or re-cultured with 10 mL of fresh LB to check whether there was any living CFU. The viability of the attached bacteria on the samples was determined by the LIVE/DEAD BacLight Viability Kit (Invitrogen). The samples were rinsed once with PBS and stained with LIVE/DEAD dye for 15 min in darkness. The pictures of the bacteria were acquired at random on a fluorescence microscope equipped with a green filter (excitation/emission, 420–480 nm/ 520–580 nm) and red filter (excitation/emission, 480–550 nm/ 590–800 nm).

2.5 Statistical analysis

With regard to the contact angle measurement, CFU counting, pH, and magnesium ion concentration measurement, each experiment was repeated 3 times and the results were shown as mean (average) ± SD (standard deviation). The data were analyzed using the t-test.

3. Results and discussion

3.1 Surface characterization

The Raman scattering spectra (Fig. 1a) acquired from the film shows

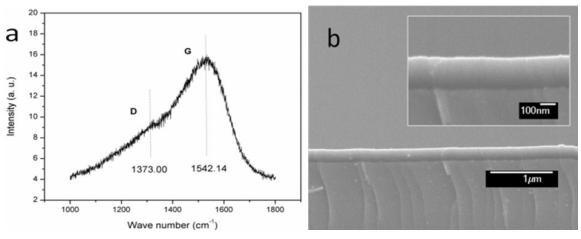

Fig. 1. Surface characterization of coated DLC film: (a) Raman spectrum of the DLC film deposited on the AZ31 alloy and (b) Cross-sectional morphology of the DLC film on the Si wafer.

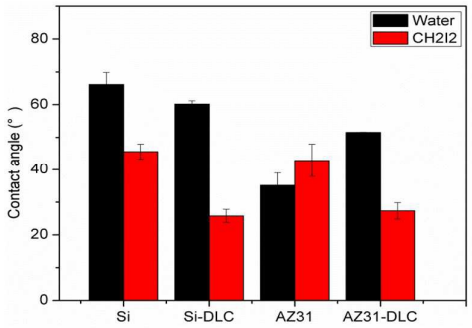

Fig. 2. Contact angles for water and CH_2I_2 on different substrates.

the typical pattern of DLC. It can be deconvoluted into two sub-peaks: G band at 1542.14 cm^{-1} and D band at 1373.00 cm^{-1} corresponding to the graphite structure and disordered graphite-like structure, respectively. The cross-sectional SEM micrograph (Fig. 1b) discloses a relatively dense and smooth film with a thickness of about 200 nm.

3.2 Hydrophilicity and surface free energy

The DLC film changes the surface hydrophilicity and free energy of the AZ31 Mg alloy. As shown in Fig. 2, the water contact angles increase from 35.1° to 51.5° but those of CH_2I_2 decrease from 42.9° to 27.3°. These results suggest that the DLC-coated surface becomes more hydrophobic than the substrate. In comparison, the contact angles on the Si-DLC for these two liquids are reduced from 66.2° to 60.2° and 45.6° to 25.8°, respectively. The surface free energy is also altered as shown in Table 1. For the AZ31 alloy, the dispersive component increases from 32.56 mN/m to 40.89 mN/m and the polar component decreases from 30.55 mN/m to 16.59 mN/m. Concerning the Si substrate, the dispersive component increases from 33.43 mN/m to 42.24 mN/m and the polar component of about 11 mN/m is almost the same. The surface free energies of AZ31 and Si become very similar (about 55 mN/m) after DLC deposition although the values of the two pristine materials are quite different.

3.3 Electrochemical study

Electrochemical measurements are conducted to evaluate the corrosion resistance of the modified AZ31 alloy. Fig. 3a displays the polarization curves and Fig. 3b presents the Nyquist plot. After plasma modification, the corrosion current density diminishes significantly from 3.17×10^{-4} A/cm^2 to 6.53×10^{-5} A/cm^2. Meanwhile, the capacitive loop observed from the treated sample is enlarged

Table 1. Surface free energies (mN/m) of different samples.

	γ_s^d	γ_s^p	γ_s
Si	33.43	11.27	44.70
Si-DLC	42.24	11.30	53.54
AZ31	32.56	30.55	63.11
AZ31-DLC	40.89	16.59	57.47

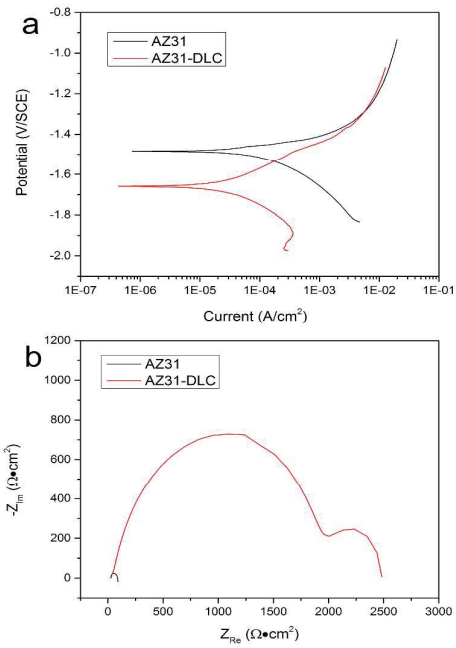

Fig. 3. (a) Polarization curves and (b) Nyquist plots of the untreated AZ31 and AZ31-DLC samples.

significantly relative to the untreated sample, suggesting that the DLC coating provides better corrosion resistance in the LB medium.

3.4 The morphology after corrosion in LB medium

The surface morphology of the AZ31 alloy and AZ31-DLC is depicted Fig. 4. After exposure to the LB medium for 6 h, severe corrosion is observed from the AZ31 sample and the cracks allow relatively easy penetration of the corrosive solution leading to further corrosion. On the contrary, corrosion takes place only in some defects on the DLC-coated surface and the other parts of the DLC surface remains intact and smooth.

3.5 pH and magnesium ion leaching

The pH values and magnesium ion concentrations in the 100 µL LB deposited on the AZ31 and AZ31-DLC samples are measured at different time points (Fig. 5). After 1 and 3 h, the pH values and the magnesium concentrations of LB medium on DLC are significantly

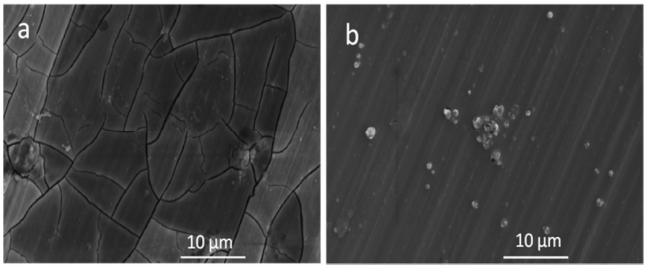

Fig. 4. Morphology of (a) AZ31 alloy and (b) AZ31-DLC after corrosion for 6 hours in 100 µl of the LB medium at 37 °C.

smaller than those on the untreated AZ31. After 6 h, the differences become less significant. The pH values of AZ31 and AZ31-DLC reach 9.51 and 9.29, respectively, and the magnesium concentrations leached from AZ31 and AZ1-DLC are 348.35 ppm and 238.05 ppm, respectively. The results are consistent with the electrochemical and morphological studies revealing that DLC improves the corrosion resistance. However, since the DLC does have some defects, leached hydroxyl and magnesium ions accumulate gradually albeit at a smaller rate after immersion for a long time.

3.6 Defects on the DLC film

To get the information about the defects, we did SEM observation of the film before corrosion, as well as 3h and 6h after corrosion. As shown in Fig. 6, there are two kinds of defects on the AZ31-DLC surface: big white "dots" (0H, 500 × magnification) and small black holes (arrows in 0H and 3H). The white dots are caused by small protrusions on the substrate that are poorly covered by DLC [23]. The black holes can be observed at 5000× magnification. After immersion for 3 h, some white dots are eroded at their edges (dashed arrows) and the black holes become larger (arrows). After immersion for 6 h, much more white dots are eroded, forming the many black rings around the white dots (6H, 500 × magnifications). Also, more black holes can be found on the surface.

3.7 CFU counting of planktonic bacteria

The planktonic bacteria CFU on the DLC-coated magnesium and Si samples are shown in Fig. 7. In the beginning, 3×10^4 bacteria CFUs

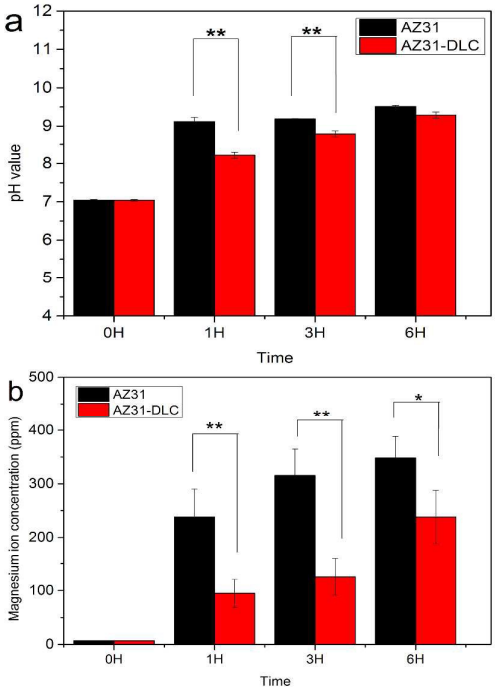

Fig. 5. (a) pH and (b) concentration of leached magnesium ions on the untreated AZ31 and AZ31-DLC samples. (**: p<0.05; *: p<0.1)

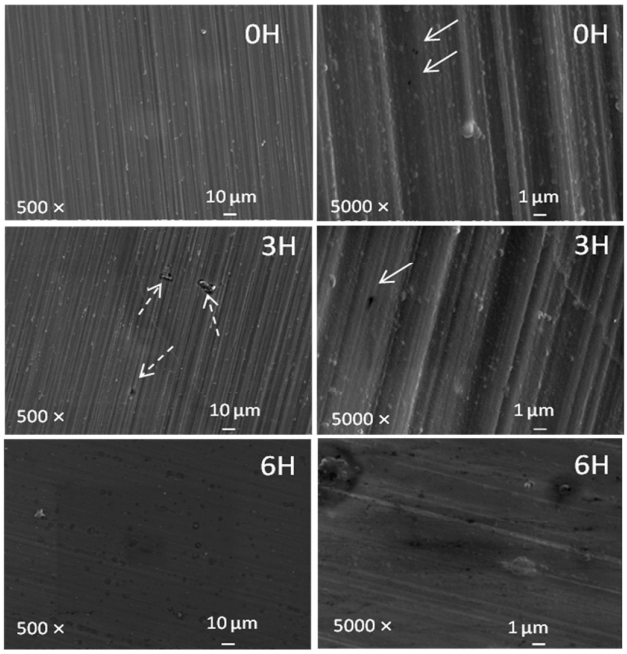

Fig. 6. SEM observation of the defects on AZ31-DLC films.

are introduced to each sample. Si and Si-DLC do not have any anti-bacterial ability and the degree of bacteria proliferation is similar to that on the culture well control. After culturing for 3 and 6 h, the CFUs are about 3×10^7 and 6×10^8, respectively. On the contrary, AZ31 and AZ31-DLC exhibit obvious anti-bacterial behaviour. After 3 h, the amount of bacteria on AZ31 is almost the same as that in the beginning due to the balance between dying and proliferation. Furthermore, the amount on AZ31-DLC has diminished to 2.3×10^2, which is two orders of magnitude smaller than that on AZ31. After 6 hours, the quantity of bacteria on AZ31 decreases to 5×10^3, but there are no living bacteria on the DLC samples. In fact, it takes the magnesium alloys up to 24 h to kill the 3×10^4 bacteria in the same

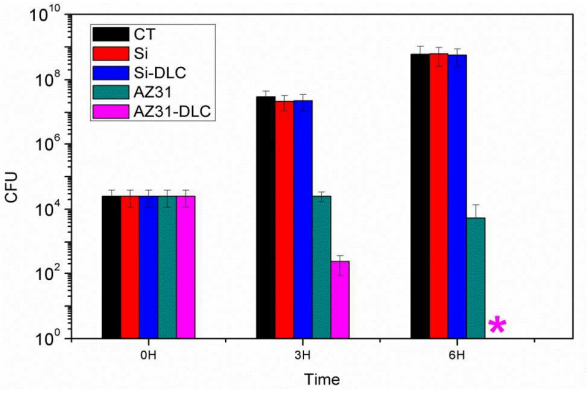

Fig. 7. Planktonic bacteria CFU after culturing in the LB medium on different substrates and DLC surfaces with bacteria cultured on 24-well plates (polystyrene) serving as the control (CT). (*: CFU = 0)

culturing conditions (unpublished data) and so AZ31-DLC has greatly enhanced anti-bacterial ability.

3.8 Adherent bacteria viability

The viability of adherent bacteria is examined using fluorescent dyes (Fig. 8). Many bacteria cells adhere to the Si and Si-DLC surfaces and they are all stained green implying that they are alive. Contrarily, only a few bacteria attach to the AZ31 surface. At the 3h time point, there are more live (green) cells than dead (red) ones and at the 6h time point, most of the attached bacteria are dead (red). In contrast, AZ31-DLC attracts the most bacteria and at the 3h time point, live and dead ones coexist as indicated by the red, green and yellow (mixture of red and green) dots in the picture. Finally, after 6 hours, all of the bacteria are stained red meaning that they are all dead.

3.9 Bacteria killing mechanism on AZ31-DLC surface

This magnesium-DLC induced anti-bacteria phenomenon is unexpected. First of all, DLC does not have bacteria killing ability as demonstrated by Si-DLC. Secondly, the DLC film which covers the magnesium substrate should weaken the inherent anti-bacterial ability of Mg. However, our results indicate otherwise. It is believed to arise from the altered hydrophilicity and free energy favoring bacteria adhesion. In fact, bacteria adhesion on the surface is a complicated process.[27] The initial step is reversible adhesion governed by physico-chemical interactions. Planktonic bacteria move to the materials due to physical forces such as Brownian motion, van der Waals force, gravitational force, hydrophobic interaction, and electrostatic attraction. The second step is irreversible adhesion by which bacteria stick to a surface by bridging the surface polymeric structures such as exopolysaccharides. Depending on the hydrophobicity of the bacteria and surfaces, bacteria adhere differently onto materials with different hydrophobicity and hydrophilic materials are more resistant to bacterial adhesion than hydrophobic materials.[28–30] In experiments conducted with different materials. [28], large quantities of bacteria attach to hydrophobic plastics with little or no surface charge, moderate numbers attach to hydrophilic metals with a positive or neutral surface charge, and very few attach to hydrophilic and negatively charged substrates. In our experiments, the DLC coating on AZ31 makes the surface more hydrophobic and so more bacteria attach to the modified surface.

The surface free energy is also important to bacteria adhesion. On the basis of the interfacial free energy balance, adhesion may be expected[31] if $\Delta F_{adh} = \gamma_{sb}-\gamma_{sl} - \gamma_{bl}<0$, where ΔF_{adh} is the interfacial free energy of adhesion, γ_{sb} is the solid-bacterium interfacial free energy, γ_{sl} is the solid-liquid interfacial free energy, and γ_{bl} is the bacterium-liquid interfacial free energy. Bacteria adhesion may decrease or increase with the surface energy of the substrate depending on the physical and chemical properties of bacteria, substrate, and media.[32] In our experiments, the surface free energy of AZ31 diminishes from 63.11 mN/m to 57.47 mN/m and so energetically, the surface is also more attractive to bacteria.

A surface favorable to bacteria adhesion normally has poor anti-bacteria ability because the bacteria can better reside and proliferate to form a biofilm. However, the DLC film on AZ31 is more effective in killing bacteria. This can be ascribed to the local release of magnesium ions and hydroxyl ions during magnesium corrosion.[33,34] Although the exact mechanism of magnesium induced bacteria inactivation has not yet been clearly elaborated, it is wide accepted that it is closely related to the degradation or corrosion process. Some researchers attribute it to the alkalinity[35,36] and others suggest that inactivation depends on the degradation rate of the alloy[4]. In our study (unpublished work), we find that the synergetic effects of both the alkalinity and magnesium ions play the inactivation role.

As shown in the schematic in Fig. 9, on the AZ31 alloy surface, corrosion occurs at a high rate and the surface is covered by the corrosion product in addition to hydrogen bubbles. The hydrogen

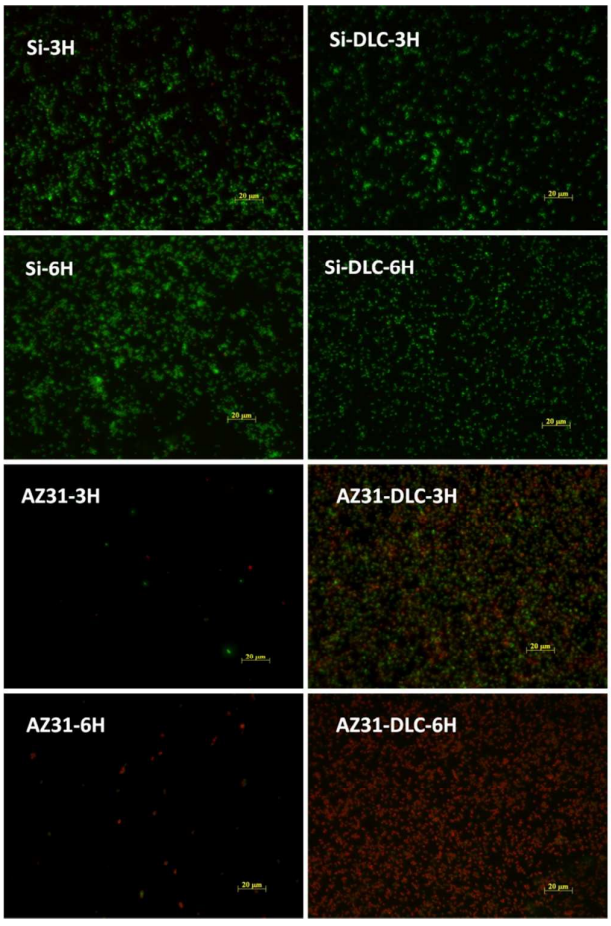

Fig. 8. Live/Dead fluorescent staining of bacteria on different substrates and DLC surfaces.

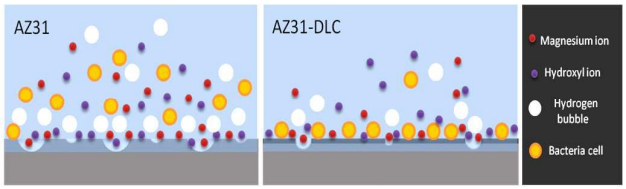

Fig. 9. Proposed anti-bacteria mechanism of the DLC film on AZ31.

bubbles rise from the bottom of the LB medium to the medium surface and then are released. The reaction and turbulence make it hard for the bacteria to adhere to the alloy surface and most of them are suspended in the medium. On the other hand, although corrosion is mitigated by DLC deposition, there are defects in the film enabling release of a small amount of magnesium and hydroxyl ions. Since most bacteria are attracted and confined on the DLC film where local release takes place, they are actually threatened by higher concentrations of magnesium and hydroxyl ions than those on the AZ31 substrate. Consequently, the bacteria are annihilated more effectively.

Conclusion

Magnesium is promising in degradable biomedical implants. In addition to the control of corrosion, the antibacterial property is crucial to prevention of infection and healing after surgery. As the inherent antibacterial ability of magnesium-based materials is closely related to the corrosion rate, our study reveals a strategy to retain the bactericidal ability without comprising the corrosion resistance by depositing DLC on AZ31 Mg alloy by one-step PIII&D. While the corrosion rate is reduced significantly, the bacteria resistance is also improved. The unexpected anti-bacteria behavior is attributed to the combined effects of favorable bacteria adhesion on the DLC surface and local release of hydroxyl and magnesium ions from the magnesium substrate *via* defects in the DLC films. The non-toxic and bactericidal Mg-DLC materials are suitable for temporary implants such as bone plates and screws. To fabricate surfaces with controllable corrosion resistance and anti-bacterial properties, defects can be intentionally and systematically introduced into the DLC coating in order to simultaneously exploit the protection offered by DLC and anti-bacterial effects rendered by the Mg alloy.

Acknowledgements

This work is supported by City University of Hong Kong Strategic Research Grant 7004188 and Hong Kong Research Grants Council (RGC) General Research Funds (GRF) Nos. CityU 112212 and 11301215.

Notes and references

1 M. P. Staiger, A. M. Pietak, J. Huadmai and G. Dias, *Biomaterials*, 2006, **27**, 1728–1734.
2 Y. Chen, Z. Xu, C. Smith and J. Sankar, *Acta Biomater.*, 2014, **10**, 4561–4573.
3 X. Gu, Y. Zheng, Y. Cheng, S. Zhong and T. Xi, *Biomaterials*, 2009, **30**, 484–498.
4 J. Y. Lock, E. Wyatt, S. Upadhyayula, A. Whall, V. Nuñez, V. I. Vullev and H. Liu, *J. Biomed. Mater. Res. - Part A*, 2014, **102**, 781–792.
5 W. Jin, G. Wu, H. Feng, W. Wang, X. Zhang and P. K. Chu, *Corros. Sci.*, 2015, **94**, 142–155.
6 C. Qi, Y.-J. Zhu, B.-Q. Lu, J. Wu and F. Chen, *RSC Adv.*, 2015, **5**, 14906–14915.
7 Z. Qiu, Y. Zhang, Y. Li, J. Sun, R. Wang and X. Wu, *RSC Adv.*, 2015, **5**, 63738–63744.
8 H. Zhao, S. Cai, Z. Ding, M. Zhang, Y. Li and G. Xu, *RSC Adv.*, 2015, **5**, 24586–24590.
9 H. Qin, Y. Zhao, Z. An, M. Cheng, Q. Wang, T. Cheng, Q. Wang, J. Wang, Y. Jiang, X. Zhang and G. Yuan, *Biomaterials*, 2015, **53**, 211–220.
10 Y. Zhao, M. I. Jamesh, W. K. Li, G. Wu, C. Wang, Y. Zheng, K. W. K. Yeung and P. K. Chu, *Acta Biomater.*, 2014, **10**, 544–556.
11 J. Robertson, *Mater. Sci. Eng. R Reports*, 2002, **37**, 129–281.
12 K. Bewilogua and D. Hofmann, *Surf. Coatings Technol.*, 2014, **242**, 214–225.
13 C. A. Love, R. B. Cook, T. J. Harvey, P. A. Dearnley and R. J. K. Wood, *Tribol. Int.*, 2013, **63**, 141–150.
14 R. Hauert, K. Thorwarth and G. Thorwarth, *Surf. Coatings Technol.*, 2013, **233**, 119–130.
15 R. W. Y. Poon, K. W. K. Yeung, X. Y. Liu, P. K. Chu, C. Y. Chung, W. W. Lu, K. M. C. Cheung and D. Chan, *Biomaterials*, 2005, **26**, 2265–2272.
16 J. Y. Chen, L. P. Wang, K. Y. Fu, N. Huang, Y. Leng, Y. X. Leng, P. Yang, J. Wang, G. J. Wan, H. Sun, X. B. Tian and P. K. Chu, *Surf. Coatings Technol.*, 2002, **156**, 289–294.
17 P. K. Chu, *Surf. Coatings Technol.*, 2010, **204**, 2853–2863.
18 G. Wu, L. Sun, W. Dai, L. Song and A. Wang, *Surf. Coatings Technol.*, 2010, **204**, 2193–2196.
19 Y. Uematsu, T. Kakiuchi, T. Teratani, Y. Harada and K. Tokaji, *Surf. Coatings Technol.*, 2011, **205**, 2778–2784.
20 J. Choi, J. Kim, S. Nakao, M. Ikeyama and T. Kato, *Nucl. Instruments Methods Phys. Res. Sect. B Beam Interact. with Mater. Atoms*, 2007, **257**, 718–721.
21 J. Choi, S. Nakao, J. Kim, M. Ikeyama and T. Kato, *Diam. Relat. Mater.*, 2007, **16**, 1361–1364.
22 N. Yamauchi, N. Ueda, a. Okamoto, T. Sone, M. Tsujikawa and S. Oki, *Surf. Coatings Technol.*, 2007, **201**, 4913–4918.
23 G. Wu, X. Zhang, Y. Zhao, J. M. Ibrahim, G. Yuan and P. K. Chu, *Corros. Sci.*, 2014, **78**, 121–129.
24 K. Baba, R. Hatada, S. Flege and W. Ensinger, *Adv. Mater. Sci. Eng.*, 2012, **2012**, 1–5.
25 D. Bociaga, P. Komorowski, D. Batory, W. Szymanski, A. Olejnik, K. Jastrzebski and W. Jakubowski, *Appl. Surf. Sci.*, 2015, **355**, 388–397.
26 F. R. Marciano, L. F. Bonetti, L. V. Santos, N. S. Da-Silva, E. J. Corat and V. J. Trava-Airoldi, *Diam. Relat. Mater.*, 2009, **18**, 1010–1014.
27 Y. H. An and R. J. Friedman, *J. Biomed. Mater. Res.*, 1998, **43**, 338–348.
28 M. Fletcher and G. I. Loeb, *Appl. Environ. Microbiol.*, 1979, **37**, 67–72.
29 a H. Hogt, J. Dankert, J. a de Vries and J. Feijen, *J. Gen. Microbiol.*, 1983, **129**, 2959–68.
30 N. Satou, J. Satou, H. Shintani and K. Okuda, *J. Gen. Microbiol.*, 1988, **134**, 1299–305.
31 H. J. Busscher, a. H. Weerkamp, H. C. van Der Mei, a. W. van Pelt, H. P. de Jong and J. Arends, *Appl. Environ. Microbiol.*, 1984, **48**, 980–983.
32 Y. Liu and Q. Zhao, *Biophys. Chem.*, 2005, **117**, 39–45.
33 G. Williams, H. N. McMurray and R. Grace, *Electrochim. Acta*, 2010, **55**, 7824–7833.

34 O. V. V Karavai, a. C. C. Bastos, M. L. L. Zheludkevich, M. G. G. Taryba, S. V. V Lamaka and M. G. S. G. S. Ferreira, *Electrochim. Acta*, 2010, **55**, 5401–5406.

35 Y. Li, G. Liu, Z. Zhai, L. Liu, H. Li, K. Yang, L. Tan, P. Wan, X. Liu, Z. Ouyang, Z. Yu, T. Tang, Z. Zhu, X. Qu and K. Dai, *Antimicrob. Agents Chemother.*, 2014, **58**, 7586–7591.

36 D. a. Robinson, R. W. Griffith, D. Shechtman, R. B. Evans and M. G. Conzemius, *Acta Biomater.*, 2010, **6**, 1869–1877.

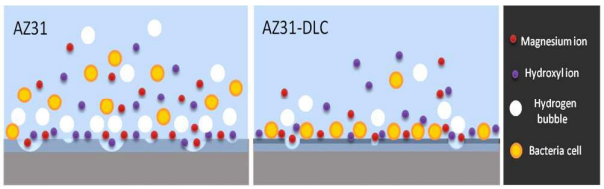

A corrosion protective DLC film is deposited on the magnesium alloy AZ31, and exhibits unusual strong anti-bacterial ability caused by the combined effects of the bacteria adhesion favorable surface and the local release of killing elements from the substrate via small defects of the DLC coating.